Ultrasound in Med. & Biol., Vol. 24, No. 6, pp. 841–854, 1998
Copyright © 1998 World Federation for Ultrasound in Medicine & Biology
Printed in the USA. All rights reserved
0301-5629/98 $19.00 + .00

PII S0301-5629(97)00210-X

● *Original Contribution*

AUTOMATIC REGISTRATION OF 3-D ULTRASOUND IMAGES

ROBERT N. ROHLING,* A. H. GEE* and L. BERMAN†
*Department of Engineering, University of Cambridge, Cambridge, UK; and †Department of Radiology, Addenbrooke's Hospital, Cambridge, UK

(*Received* 6 *June* 1997; *in final form* 13 *August* 1997)

Abstract—One of the most promising applications of 3-D ultrasound (US) lies in the visualisation and volume estimation of internal 3-D structures. Unfortunately, artifacts and speckle make automatic analysis of the 3-D data sets difficult. In this study, we investigated the use of 3-D spatial compounding to improve data quality, and found that precise registration is the key. A correlation-based registration technique was applied to 3-D ultrasound data sets acquired from *in vivo* examinations of a human gall bladder. We found that the registration technique performed well, and visualisation and segmentation of the compounded data were clearly improved. We also demonstrated that an automatic volume estimate made from the compounded data (13.0 mL) was comparable to a labour-intensive manual estimate (12.5 mL). In comparison, automatic estimates of uncompounded data are less accurate (ranging from 13.5 mL to 16.7 mL). The registration technique also has applications in intra- and interpatient comparative studies. © 1998 World Federation for Ultrasound in Medicine & Biology.

Key Words: **3-D ultrasound imaging, Registration, Spatial compounding, Volume estimation.**

INTRODUCTION

3-D ultrasound is a new imaging modality that has already been recognised as a valuable tool for a variety of clinical applications. Conventional 2-D diagnostic imaging is performed with a hand-held probe that transmits ultrasound pulses into the body and receives the echoes. The magnitude and timing of the echoes are used to create a 2-D grey-level image (B-scan) of a cross-section of the body in the scan plane. 3-D ultrasound extends this concept so that volumes of intensity data are created from pulse-echo information.

Unfortunately, high-quality instantaneous 3-D imaging remains a long-term research goal. One promising approach centers around the development of a new type of phased array probe that sends and receives echoes from a 2-D array of elements (instead of the usual 1-D array). However, several technical challenges must be overcome before such probes receive clinical acceptance (Smith et al. 1995). Alternative approaches that make use of conventional 2-D ultrasound technology include the freehand and swept-volume techniques (Deng et al. 1996; Fenster and Downey 1996; Steiner et al. 1994). Instead of taking an instantaneous 3-D snapshot, these techniques construct a 3-D data set from a number of 2-D B-scans acquired in rapid succession. In the freehand paradigm, a 3-D position sensor is attached to the probe, so that each B-scan can be labelled with the position and orientation of the scan plane (see Fig. 1). Subsequent processing can build up a 3-D description of the imaged anatomy, in much the same manner as is possible with CT (computed tomography) or MRI (magnetic resonance imaging), but with less expensive and less invasive technology. Swept-volume systems are similar, but employ a specially constructed probe to mechanically sweep the B-scans through a volume of interest. In this study, we focused on the freehand technique. Both the swept-volume and freehand techniques have been successfully applied to a number of clinical problems. These include imaging of the fetus (Chervenak et al. 1993), vascular structure (Franceschi et al. 1992), gall bladder (Fine et al. 1991), breast (Moskalik et al. 1995), kidney (Gilja et al. 1995), and heart (Salustri and Roelandt 1995). In review articles about 3-D ultrasound (Fenster and Downey 1996; Hottier and Collet Billon 1990), the authors suggest that 3-D visualisation and volume estimation are among its most attractive capabilities. Unfortunately, standard visualisation and analysis programs (designed primarily for MRI and CT images) often yield unsatis-

Address correspondence to: Robert N. Rohling, Department of Engineering, University of Cambridge, Trumpington Street, Cambridge CB2 1PZ UK. E-mail: rnr20@eng.cam.ac.uk

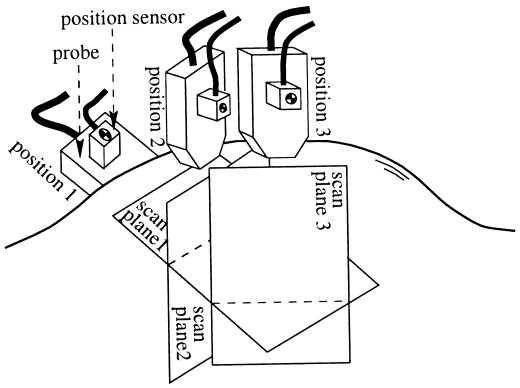

Fig. 1. 3-D freehand ultrasound imaging. Freehand imaging allows the physician to move the probe as in a normal ultrasound examination. The position sensor measures the position and orientation of each scan plane. Note that the planes intersect each other.

factory results with 3-D ultrasound. There are a number of properties of ultrasound data that make visualisation and volumetric data analysis difficult (Sakas et al. 1995). Several of the items in the following list are illustrated in Fig. 2:

- Significant noise and speckle (speckle arises from the constructive-destructive interference of the coherent ultrasound pulses)
- lower dynamic range than MR and CT images
- blurred boundaries around anatomical features
- boundaries with varying intensities caused by changes in surface curvature and orientation
- partially or completely shadowed surfaces from objects nearer the probe;
- variable resolution through the volume, dependent on both the spacing between the B-scans and the location within a B-scan.

In response to these problems, considerable effort has gone into the development of new segmentation and visualisation techniques for ultrasound data. Although some success has been achieved for special cases, such as fetal imaging (Sakas et al. 1995), fast and fully automatic generic techniques remain elusive. Our aim was to exploit spatial compounding to improve the quality of the 3-D ultrasound data, so that existing visualisation and analysis techniques would be more successful.

The principle of spatial compounding is to image the region of interest (ROI) repeatedly, from different look directions (also called isonation angles), and then average the values from the intersecting B-scans when constructing the 3-D data set (see Fig. 3). The speckle signal, which decorrelates from different look directions, is suppressed by the averaging operation. Conversely, real anatomical features (tissue boundaries, for example) will be observed in the same location from all look directions. Provided the registration of the scan planes is accurate, the averaging operation will highlight the real anatomical features. Furthermore, the variety of look directions ensures that boundaries become more homogeneous and continuous, and shadowed regions are filled in.

Every freehand system has to deal with compounding in some manner, because it is almost inevitable that the scan planes intersect. In this paper, we propose deliberate, extensive compounding, with the aim of producing high-quality 3-D data sets that lend themselves to clear visualisation and accurate volumetric analysis. Spa-

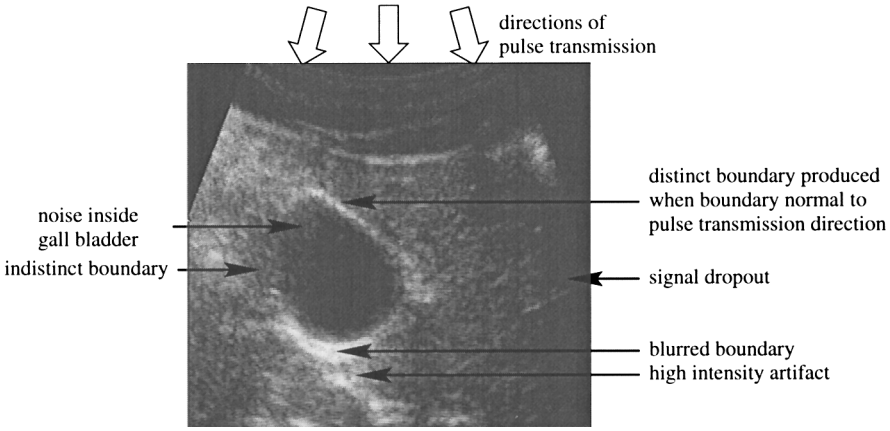

Fig. 2. B-scan of a human gall bladder. The gall bladder is the dark circular region just left of center. Most of the properties of ultrasound that inhibit automatic analysis are present in this image. In particular, the speckle phenomenon is visible as a granular texture throughout the image. The intensity of the gall bladder boundary varies around its length. Sections of the boundary that are perpendicular to the pulse transmission direction produce high-intensity echoes, and sections that are parallel produce low-intensity echoes.

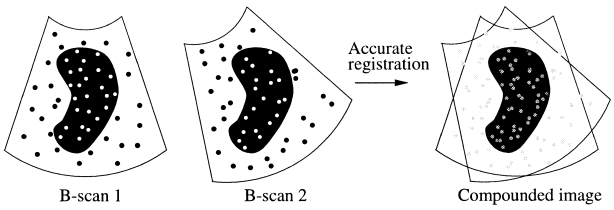

Fig. 3. Spatial compounding. This is a simple illustration of 2-D spatial compounding. Two scans of the same plane are accurately registered and then averaged together to produce a compounded image with an improved SNR. The principle extends to 3-D, where compounding can be performed wherever scan planes intersect (see Fig. 1).

tial compounding can also be performed on data gathered by 2-D array or swept-volume systems. The only requirement is that the volume of data is reconstructed from pulse-echo information originating from different look directions. Two volumes of data acquired from similar look directions will not produce improved compounded images because no new information is available.

Although a considerable amount of research has been performed on spatial compounding of 2-D ultrasound images, we are aware of only two published articles on 3-D spatial compounding. In the first article (Moskalik et al. 1995), two 3-D data sets were registered using manual landmark matching. This constitutes a labour-intensive solution to a specific registration problem. The second article (Nelson and Pretorius 1994) cited the improvements made possible by 3-D compounding, but simply stated the need for accurate registration without providing further detail.

Indeed, the key to effective spatial compounding is to achieve a sufficiently high registration accuracy. Registration errors will place the same anatomical feature seen from different look directions at different positions in the reconstructed volume. This phenomenon will result in a blurring of the imaged features. Although the largest sources of registration error are likely to be from inaccurate B-scan position measurement and tissue motion during the scan, refraction of the ultrasound beam and other imaging effects also contribute (Wells 1993). In practice, the accumulated error is significant and it is, therefore, necessary to use image-based registration techniques to achieve the required level of accuracy.

We have already completed a pilot study into spatial compounding with image-based registration (Rohling et al. 1997). The study used an organ phantom (an artificial object that mimics the properties of an internal organ) to demonstrate that the registration errors can be corrected. We also showed that the SNR of the images increases with the square root of the average number of B-scans intersecting each voxel (in agreement with statistical theory). Furthermore, segmentation and volume estimates are improved by spatial compounding.

To continue this line of research, it was necessary to redesign the freehand acquisition system so that B-scans could be grabbed at the full video frame rate. This allows a heavily compounded data set to be acquired in the course of a short examination. This paper presents the first results of *in vivo* examinations using the new acquisition system.

METHOD

3-D reconstruction

The freehand acquisition system comprises an ultrasound scanner, a standard probe and a position sensor. A Toshiba model SSA-270A/HG (Toshiba American Medical Systems, Tustin, California) scanner was used with a 3.75-MHz convex curvilinear array probe. The position and orientation of each scan plane, relative to a fixed transmitter, were measured by an AC magnetic field receiver (Polhemus FASTRAK, Polhemus Incorporated, Colchester, Vermont) mounted on the probe. Images from the scanner were recorded by an 8-bit frame grabber at a rate of 25 frames/s. The images and the position data were stored in the memory of a Silicon Graphics Indy workstation, Silicon Graphics Corporation, Mountain View, California. The set of acquired

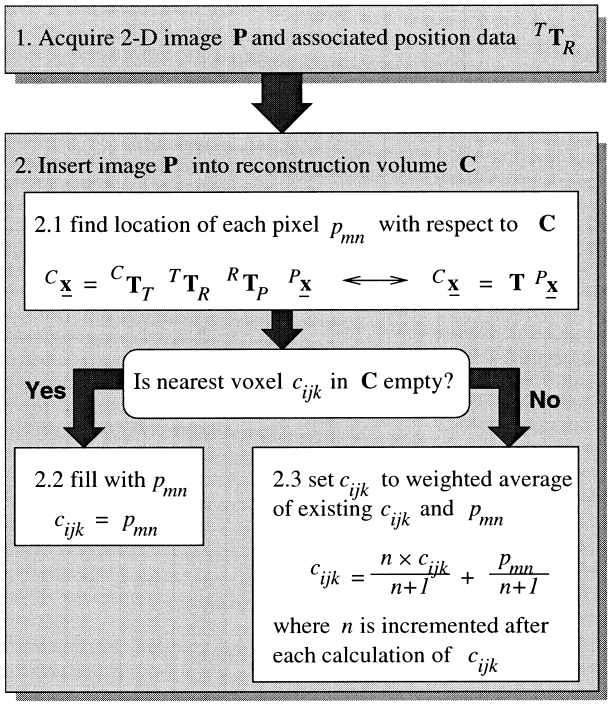

Fig. 4. Reconstruction algorithm. Steps 1 and 2 are repeated for all images acquired in an examination.

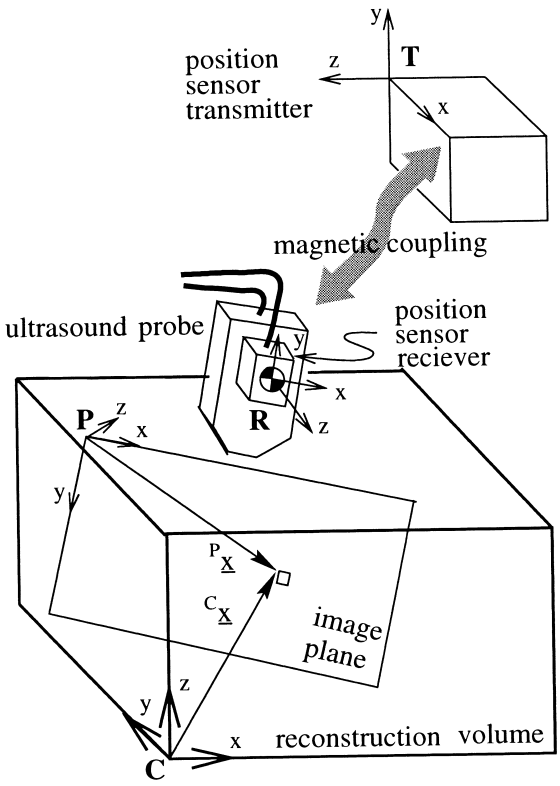

Fig. 5. Coordinate systems used for reconstruction. The following notation is used to label coordinate systems: **T** = transmitter; **C** = cuberille; **P** = plane; and **R** = receiver.

B-scans was then used to reconstruct a regular 3-D data set, as required by most visualisation and data analysis software packages. The reconstruction algorithm is illustrated in Fig. 4, with a detailed description following below.

Each B-scan is represented as a 2-D array **P** of intensities p_{mn}. The reconstruction volume takes the form of a 3-D voxel array (or cuberille) **C**. Each element c_{ijk} of **C** represents a voxel in space. The voxel size is chosen *a priori*: small voxels (though no smaller than the pixel dimensions) produce high-resolution reconstructions, larger voxels produce lower-resolution reconstructions. Although high-resolution reconstructions reveal more detail, they also require considerable computational resources to generate and manipulate. There is a fundamental tradeoff between ease of data manipulation and resolution.

Figure 5 depicts the 4 coordinate systems used for reconstruction. The position sensor measures the relative position and orientation of the receiver with respect to the transmitter. These measurements are converted into a 4×4 homogeneous transformation matrix. A standard notation is used to describe ${}^{T}\mathbf{T}_{R}$ as the transformation from the coordinate system at the receiver (R) to the coordinate system at the transmitter (T).

The position of a pixel p_{mn} with respect to its plane (P) is expressed as a homogeneous vector ${}^{P}\mathrm{x}$. The pixel position, with respect to the cuberille coordinate system (**C**), can be determined by transformation to the receiver coordinate system, then to the transmitter and, finally, to the reconstruction volume via ${}^{R}\mathbf{T}_{P}$, ${}^{T}\mathbf{T}_{R}$ and ${}^{C}\mathbf{T}_{T}$, respectively. ${}^{C}\mathbf{T}_{T}$ describes the transformation from the transmitter to the corner of the cuberille. It is set to the limits of the reconstruction volume that the physician scans and remains constant throughout the reconstruction. ${}^{R}\mathbf{T}_{P}$ describes the transformation between the corner of the scan plane and the coordinate system of the receiver. It also remains constant throughout the reconstruction and is determined by calibration. The cumulative matrix multiplication of ${}^{C}\mathbf{T}_{T}\ {}^{T}\mathbf{T}_{R}\ {}^{R}\mathbf{T}_{P}$ is abbreviated to **T**.

Determination of ${}^{R}\mathbf{T}_{P}$ is performed using a calibration rig comprising 3 orthogonal wires mounted in a water bath (Carr 1996). The 3 wires are scanned separately from a variety of look directions. The orthogonality of the wires can be used to write one equation in ${}^{P}\underline{\mathbf{x}}$, ${}^{T}\mathbf{T}_{R}$ and ${}^{R}\mathbf{T}_{P}$ for each B-scan. To improve the accuracy of the calibration, it is advantageous to acquire more B-scans than are necessary to determine the 6 parameters of ${}^{R}\mathbf{T}_{P}$, and use an iterative least squares algorithm to solve the overdetermined problem. Studies have shown this method to be accurate to 1 mm (Carr 1996).

Before the start of the examination, the voxels in the reconstruction volume are all set to zero. As each B-scan is acquired, each voxel c_{ijk} is adjusted according to the

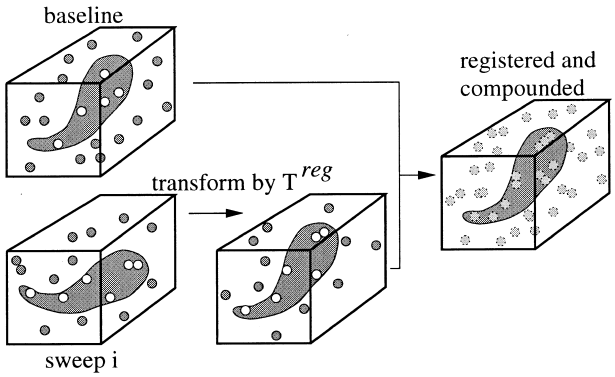

Fig. 6. Registration and spatial compounding of noisy 3-D data. The first sweep is called the baseline because all other sweeps are registered to it. $\mathbf{T}^{reg}$ is the homogeneous transformation matrix describing the rigid body registration. Transformation of Sweep i by $\mathbf{T}^{reg}$ aligns it with the baseline data so that compounding can be performed with minimal loss of spatial detail. Because Sweep i is reconstructed from B-scans taken from different look directions to the baseline B-scans, the noise is uncorrelated. Compounding the two registered data sets therefore reduces the level of noise.

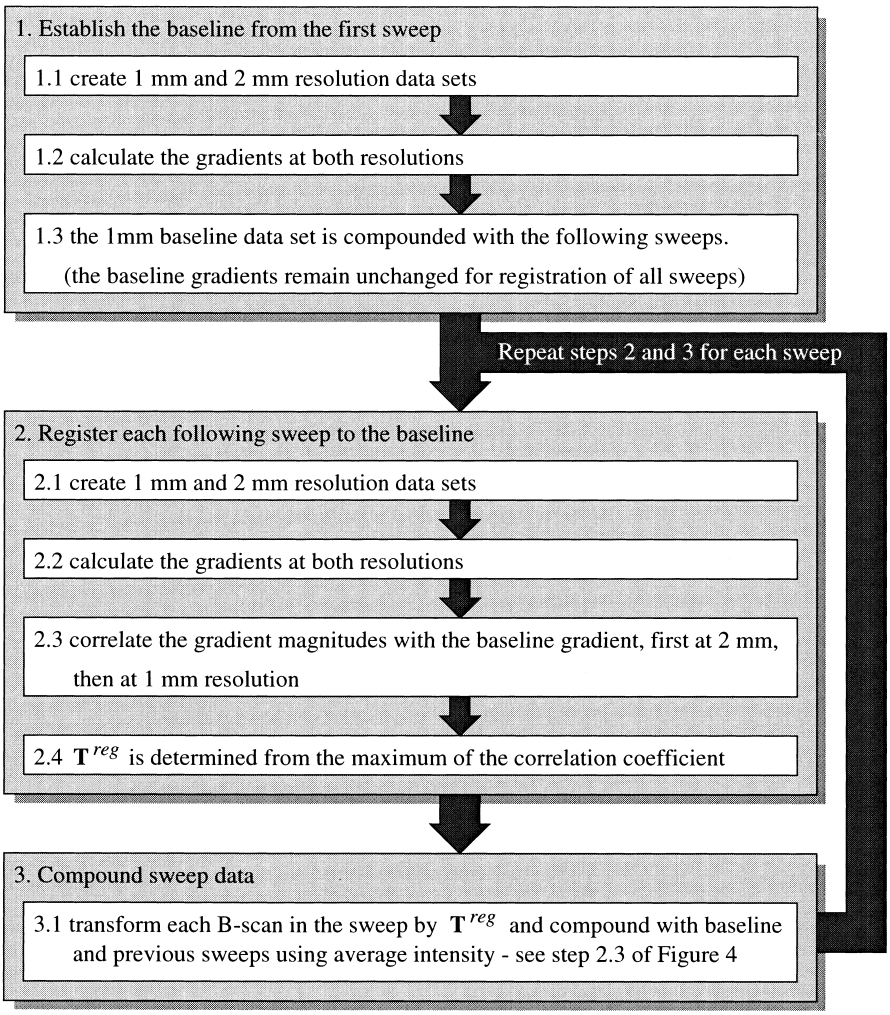

Fig. 7. Algorithm for registration and compounding of multiple sweeps.

pixels p_{mn} that intersect it. A single voxel will envelop many pixels if the voxel size is larger than the B-scan pixel size. Each voxel may also be intersected again by future B-scans. These possibilities are dealt with by step 2.3 of the reconstruction algorithm in Fig. 4, which describes a compounding operation to average all pixels that intersect a voxel. After a substantial portion of **C** is filled, it can be displayed on a computer monitor by several different methods, including surface rendering and any-plane slicing. Hereafter, the term slice is used to indicate an image produced by any-plane slicing.

3-D registration: background and theory

In a typical *in vivo* 3-D ultrasound examination, the physician scans smoothly and continuously a region of interest from one extent to the other. Each sweep of the region can be used to reconstruct a 3-D data set. The look direction of the probe (*i.e.*, window location and isonation angle) is changed slightly between each sweep so that different views of the region are obtained.

The basic idea of spatial compounding is to combine the data from the individual sweeps into a single 3-D data set. If no errors are present, the sweeps can be combined using only the position sensor readings. The manufacturer states that the RMS (root mean squared) accuracy of the FASTRAK position measurements is 0.8 mm, with a resolution of 0.38 mm. The angle measurements are stated to have an RMS accuracy of 0.15 degrees with a resolution of 0.025°. However, the accuracy of imaging a point is determined by the accumulated sources of error at each stage of the data-acquisition process, including the speed-of-sound estimate, the FASTRAK readings and the calibration of the FASTRAK receiver to the plane of the B-scan. In practice, therefore, image-based registration is required to align the sweeps.

Spatial compounding is performed by accurately

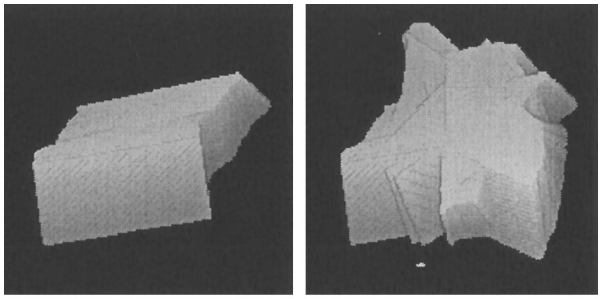

(a) single sweep (b) compounded

Fig. 8. Volume of reconstruction filled by sweeps: (a) Volume of the reconstruction filled by the baseline Sweep 0; (b) volume filled by Sweeps 0 to 5. Note how the volume is enlarged by compounding because the individual sweeps only partially overlap each other.

registering the subsequent sweeps to the first baseline sweep. Even though some nonrigid organ motion is undoubtedly present, we have found that the majority of the registration errors are caused by inaccurate position measurements and can be corrected by rigid body transformation (Rohling et al. 1997). The exception is when imaging pulsatile blood flows, when it is generally necessary to gate the B-scan acquisition to an ECG signal (Deng et al. 1996; Salustri and Roelandt 1995). The registration process is illustrated in Fig. 6.

There has been considerable research into the automatic registration of CT and MR images, but very few attempts to apply these techniques to 3-D ultrasound. Cmprehensive surveys of the various registration techniques are presented by Taylor et al. (1996) and van den Elsen et al. (1993). We evaluated a number of the more popular approaches on the ultrasound data, with varying degrees of success.

The first class of techniques we tested were those based on landmark matching. The difficulty with these techniques lies in identifying suitable landmarks to match. For example, if it were possible to extract the organ boundaries from two data sets, it would be feasible to manually align the two surfaces (given suitable visual feedback). However, it is precisely because such features are difficult to extract from ultrasound data that we are attempting registration and compounding. Even with

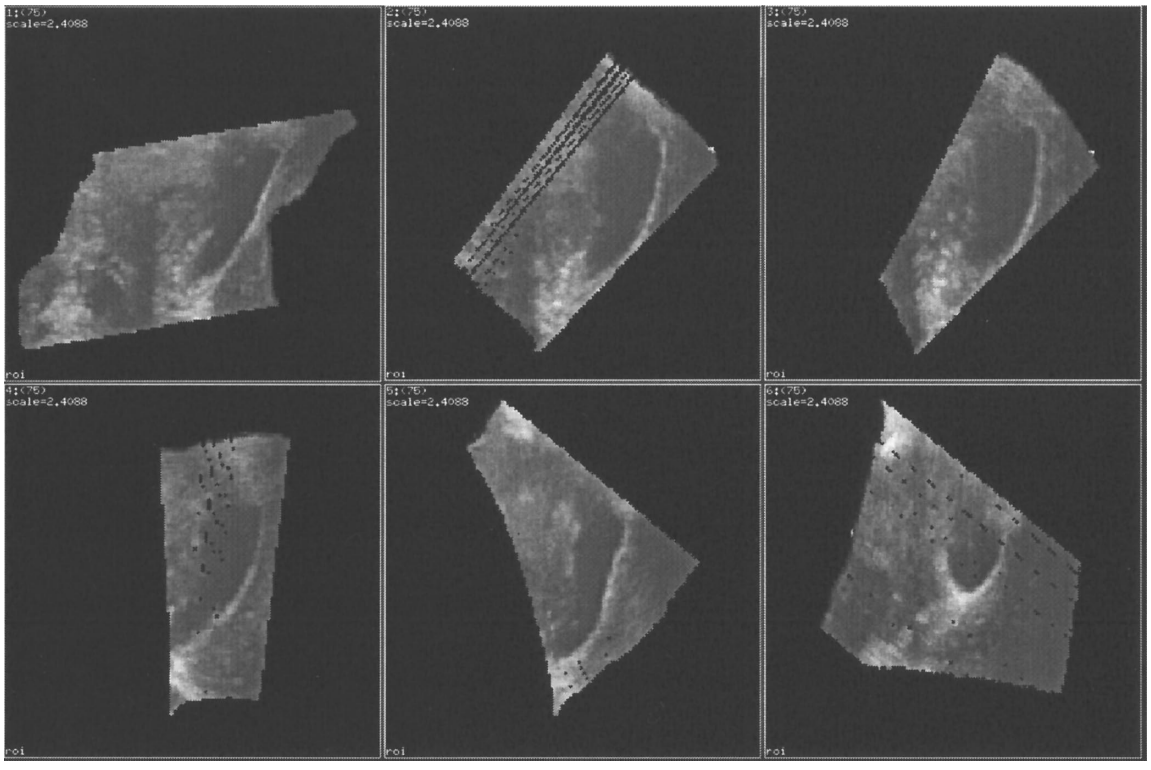

Fig. 9. Slices of reconstructions of individual sweeps before registration. Sweeps 0 to 5 are shown in two rows, starting from top left. All slices were taken at the same location in the reconstruction, identical to the locations used in Figs. 10 and 12. The data has not undergone any processing, so gaps remain in some reconstructions where the B-scans are widely spaced. The cross-sections of the gall bladder appear differently in each sweep, indicating significant registration errors.

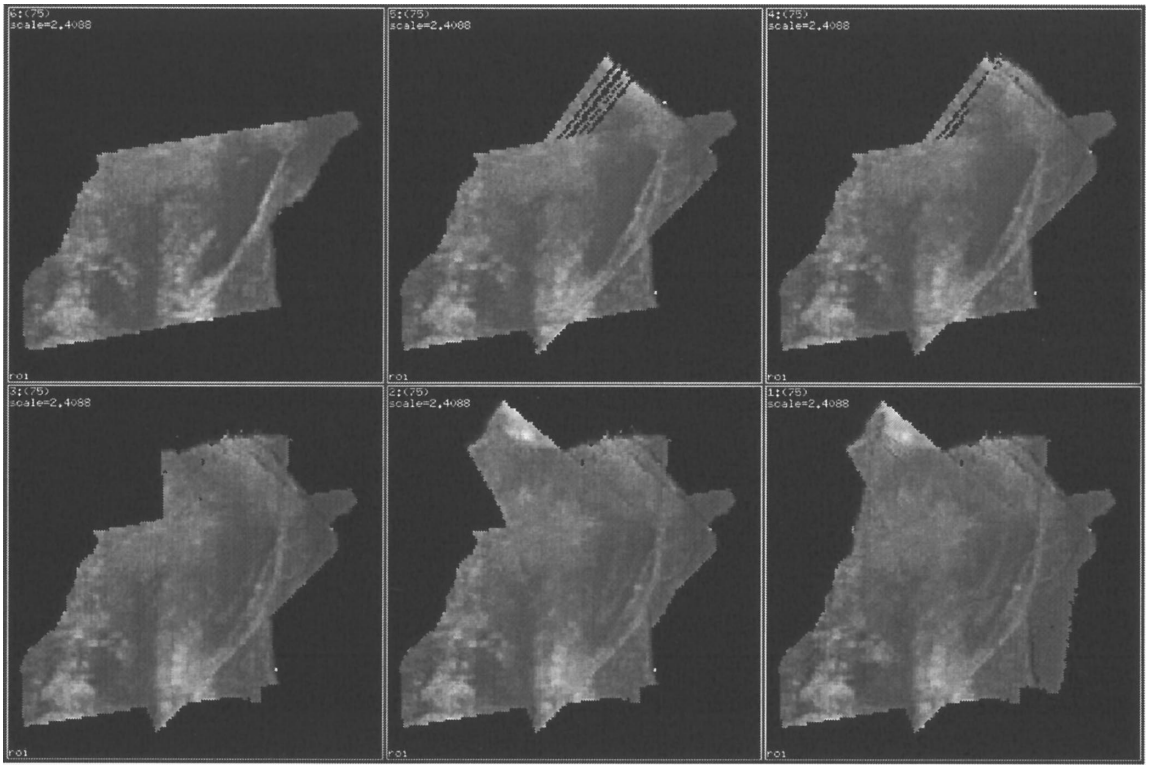

Fig. 10. Slices of compounded reconstructions before registration. Slices of reconstructions compounded incrementally with Sweeps 0 to 5 are shown in two rows, starting from top left. All slices were taken at the same location in the reconstruction volume, identical to the locations used in Figs. 9 and 12. As more and more sweeps are compounded together using the position sensor data alone, the gall bladder becomes more blurred and eventually indistinguishable. Image-based registration is therefore required for accurate spatial compounding.

suitable surfaces to align, the manual approach is not sufficiently accurate to produce sharp, compounded data.

More accuracy is possible with assisted, point-based landmark matching. In this paradigm, the user identifies matching points in the two data sets, and then the transformation which brings one set of points into close alignment with the other is computed. The problem with this approach is the difficulty in identifying distinguished points on smooth organ boundaries. Other landmark-based approaches include automatic surface-surface matching (Levine et al. 1988) and automatic curve-curve matching (Thirion et al. 1992). However, all such techniques rely on the accurate extraction of suitable features to match, which is generally not feasible in ultrasound images.

The second broad class of registration techniques makes use of some sort of correlation measure. Such techniques have been found to be robust for multimodal (MRI to CT) registration (Maintz et al. 1996; van den Elsen et al. 1995). No user interaction, explicit segmentation or landmark identification is required. High accuracy can be achieved through a coarse-to-fine search, and it is possible to register 3-D data sets that are only partially overlapping. Registering two 3-D ultrasound data sets has much in common with registering an MR data set to a CT one: in both cases, the data sets to be aligned can appear substantially different, although sharing some common features. For this reason, we chose to investigate correlation-based registration of each sweep onto the baseline.

3-D registration: correlation-based technique

Two volumes of intensity data can be registered by searching the transformation parameter space for a peak in the correlation function. In the current application, we are only considering rigid body transformations, so the parameter space is 6-dimensional (3 translations and 3 rotations). For two volumes, L_1 and L_2, the correlation coefficient is:

$$\mathrm{corr}(\underline{\mathbf{a}}) = \sum_{(x,y,z)\epsilon L_1} L_1(x,y,z)\, L_2(\mathbf{T}_a(x,y,z)) \qquad (1)$$

where $\underline{\mathbf{a}}$ is the vector of the registration parameters, and $\mathbf{T_a}$ is the rigid body transformation matrix corresponding to $\underline{\mathbf{a}}$.

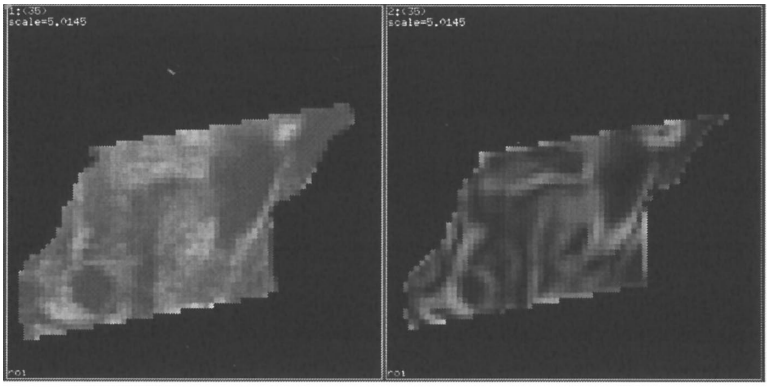

(a) 2 mm resolution

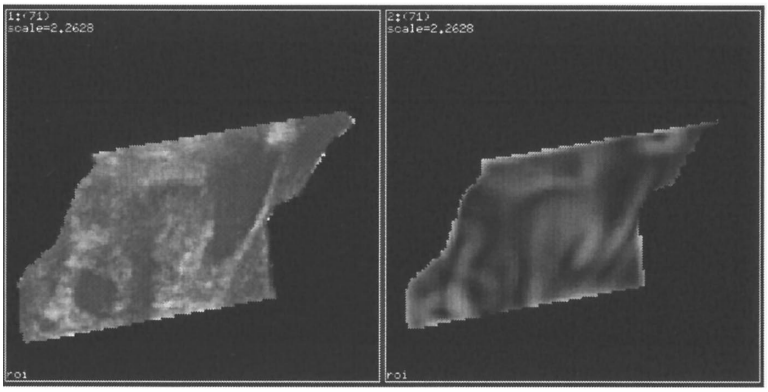

(b) 1 mm resolution

Fig. 11. Differential geometric features used for registration. The left images are slices of the original data and the right are the magnitudes of the 3-D gradient. The features used for correlation at 2-mm resolution are shown in (a), and the features used for correlation at 1-mm resolution are shown in (b).

It remains to decide what features of the data sets to correlate. Because different ultrasound images of the same anatomy can appear substantially different (as explained in the Introduction), simple correlation of the raw intensity data is not likely to succeed. Again, we look to multimodal MR-CT registration for inspiration. Raw MR

Table 1. Registration errors.

	Registration error					
Sweep	x (mm)	y (mm)	z (mm)	α (degrees)	β (degrees)	γ (degrees)
1	−2.0	9.0	0.0	−6.3	−1.7	0.6
2	−3.0	16.0	−4.8	−10.9	−3.4	2.3
3	1.0	−2.0	−9.0	−5.2	−8.6	−2.3
4	0.0	8.7	−16.0	−2.8	−6.9	4.6
5	10.0	−12.0	−10.0	6.9	−8.0	−3.4

The six parameters of $\mathbf{T}^{reg}$ are listed. Translation is expressed as x, y, z and rotation about the z, y and x axes as α, β and γ, respectively.

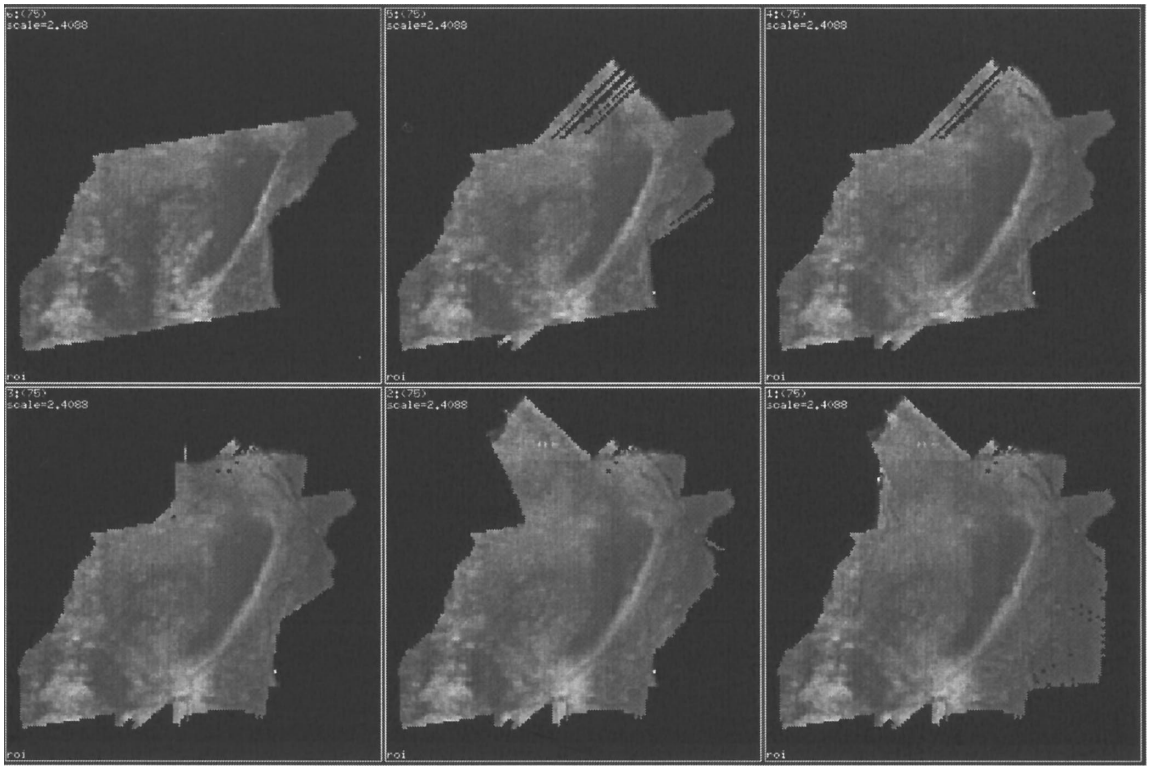

Fig. 12. Slices of compounded and registered reconstructions. Slices of reconstructions compounded incrementally with Sweeps 0 to 5 are shown in two rows, starting from top left. All slices were taken at the same location in the reconstruction volume, identical to the locations used in Figs. 9 and 10. The registration has aligned the organ boundaries in the individual sweeps, so the fully compounded data set retains the original organ shape. Compounding has also reduced speckle noise and made the gall bladder more distinct.

and CT data sets cannot be compared directly, yet they share some common features that can be usefully correlated. For example, differential operators such as edge and ridge detectors can transform MR and CT scans of the skull into comparable data sets (Maintz et al. 1996).

In a recent comparative study of multimodal 3-D

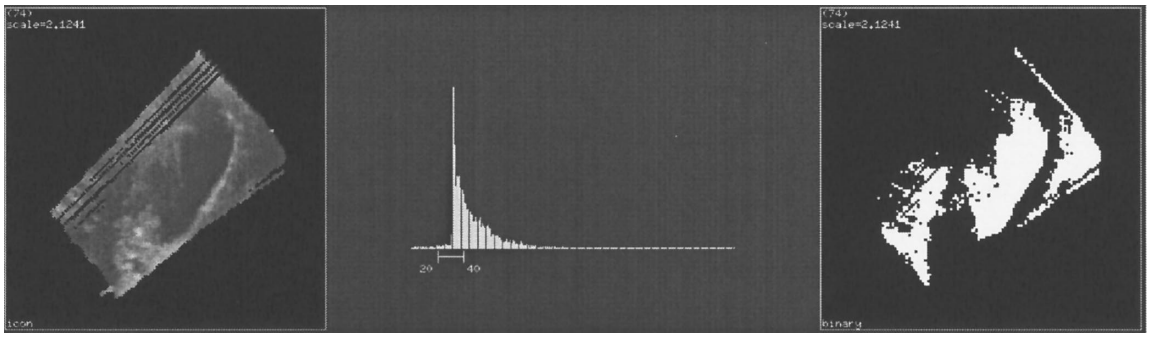

Fig. 13. Threshold segmentation of reconstructions from a single sweep. A slice of the reconstruction from Sweep 1 is shown on the left, identical to the location used in Fig. 14. The slice's grey-level histogram is shown in the middle. The data has not undergone any processing. The segmentation by thresholding the intensities within the range [20, 40] is shown on the right. The problem with segmentation of ultrasound data by thresholding is that the organ is not easily isolated from the surrounding noise and artifacts. In this case, the image has a dark region from signal dropout near the gall bladder, which affects the segmentation. A narrower threshold range reduces the volume outside the gall bladder that falls within the range, but also creates gaps within the gall bladder. The range of [20, 40] represents the best tradeoff between the two throughout the reconstruction.

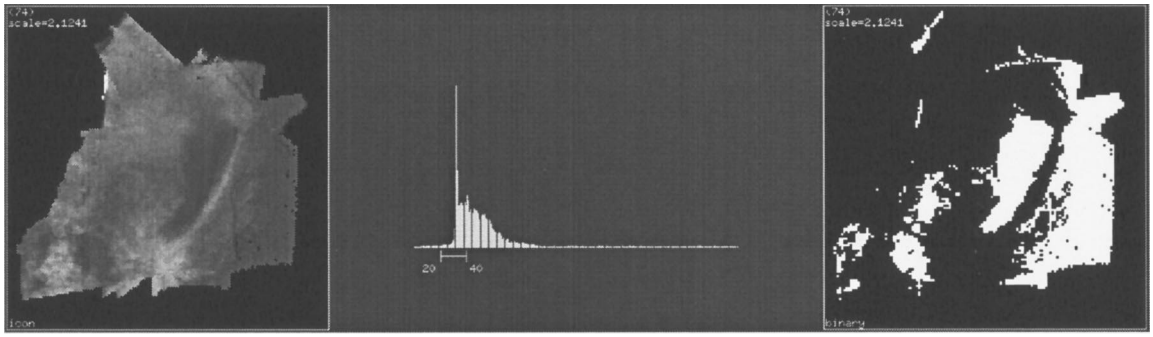

Fig. 14. Threshold segmentation of compounded reconstruction. The segmentation has been performed in an identical manner to Fig. 13, yet the segmentation is more accurate.

image registration (Maintz et al. 1996), correlation of the magnitude of the 3-D gradient was found to give the best performance. The 3-D gradient magnitude is invariant under the group of orthogonal transformations (translation, rotation, and reflection), and tends to produce better results than Laplacian and ridgeness operators (Maintz et al. 1996). For this reason, we attempted to register the ultrasound sweeps by correlating the 3-D gradient magnitudes of the data sets. The gradients are calculated by convolution of the 3-D data set with the derivative of a 3-D Gaussian kernel. When applied to ultrasound data, the gradient magnitude operator produces a transformed image with local maxima near organ boundaries. We calculated the gradients efficiently using a separable, recursive algorithm (Monga et al. 1991).

The main drawback of all correlation-based registration techniques is the significant computational expense of the search over the 6-D parameter space. However, considerable savings are possible using a multiresolution approach (van den Elsen et al. 1995). A multiresolution pyramid is constructed with the original data set at the base. Each higher level is produced at half the resolution of the previous level. The pyramid continues until the largest structures are no longer discernible. The basic idea is that wide range searches can be performed efficiently near the top of the pyramid and narrow, but accurate, searches at the bottom. Results from the searches at each level provide initial search locations at lower levels until the bottom of the pyramid is reached.

Because the position sensor readings provide a fairly good initial guess at the correct registration, only two pyramid levels are required. Our final reconstructions use 1 mm voxels, so searches started with a resolution of 2 mm.

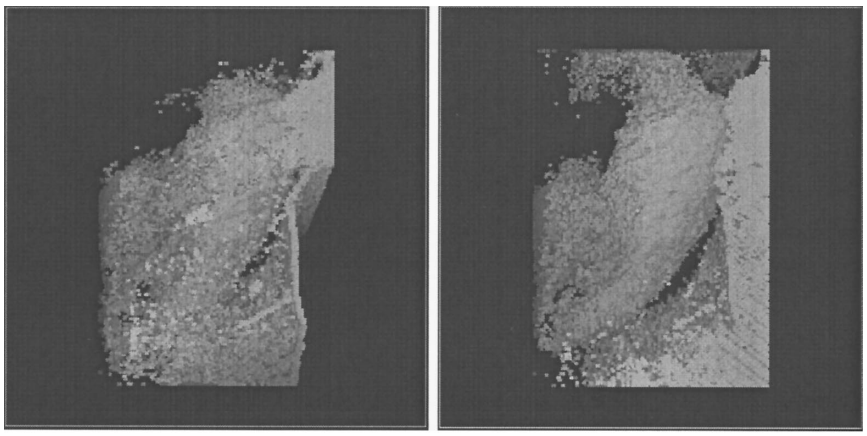

(a) single sweep (b) compounded

Fig. 15. 3-D segmentation of unprocessed data. Surfaces are extracted by thresholding, similar to the method illustrated in Figs. 13 and 14. No other data processing has been performed. Spatial compounding clearly suppresses the noise, making the surface easier to detect.

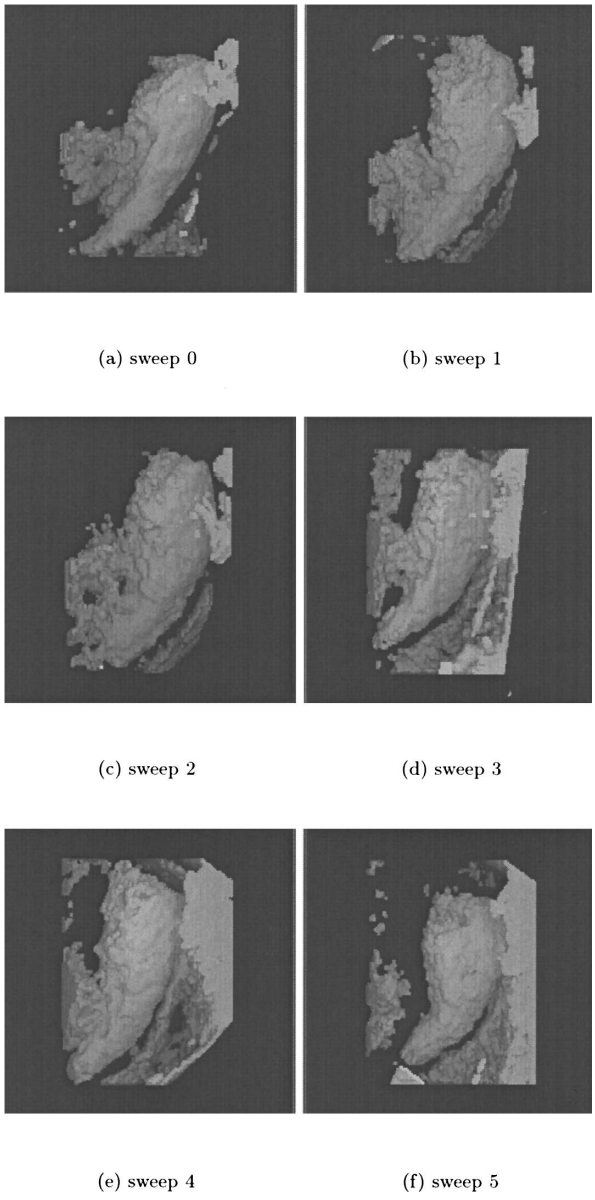

(a) sweep 0 (b) sweep 1

(c) sweep 2 (d) sweep 3

(e) sweep 4 (f) sweep 5

Fig. 16. 3-D segmentation of individual sweeps after data processing. The reconstructed 3-D data sets are interpolated to fill gaps, and Gaussian filtered to remove speckle. Segmentation is then performed by thresholding the processed data. All images were produced with identical filter sizes, interpolation parameters and threshold ranges. Compared with Fig. 15a, a considerable amount of noise has been removed by processing. In each sweep, however, the gall bladder is not disconnected from the surrounding noise and artifacts.

The correlation coefficient is sufficiently well-behaved to allow two searches, with different step sizes, at each level of the pyramid. So two searches were performed at the 2-mm resolution; the first with large steps to cover a large part of the parameter search space, the second with smaller steps around the first correlation peak. The maximum of the 2-mm search is then used as the center of the search at the 1-mm resolution where, again, two searches are performed. Because the initial guess is close to the optimal registration, local minima are not encountered.

$\mathbf{T}^{reg}$ is constructed from the parameter values corresponding to the maximum correlation coefficient. To compound the registered sweep i with the baseline data, each B-scan of sweep i undergoes the additional transformation $\mathbf{T}^{reg}$ (as in step 2.1 of Fig. 4):

$$ {}^{C}\underline{\mathbf{x}} = \mathbf{T}^{P}\underline{\mathbf{x}} \rightarrow {}^{C}\underline{\mathbf{x}} = \mathbf{T}^{reg}\mathbf{T}^{P}\underline{\mathbf{x}} \qquad (2) $$

An overview of the compounded reconstruction algorithm, using the correlation-based registration method, is given in Fig. 7.

Experiments

For this study, we examined the gall bladder of a healthy human subject. The gall bladder can be scanned from a number of different look directions, each giving a slightly different view. The variety of look directions used in this study is apparent in Fig. 8a, b.

The subject was requested to lie motionless on a bed and to breathe lightly to minimise motion-induced errors during scanning. Approximately 100 B-scans are required to cover the gall bladder from tip to tail with sufficient resolution to fill a data set with 1-mm voxels without gaps. Because our acquisition system records B-scans at 25 frames/s, 600 B-scans can be acquired in only 24 s. This allows 6 sweeps of the organ during that time.

Because all 6 sweeps are acquired in a single examination, the B-scans must be grouped into coherent sweeps. The gall bladder examination was easily partitioned by manually reviewing the B-scans in the order of acquisition. Software is currently being developed to allow the physician to start and stop acquisition using a touch-sensitive display. This will allow the physician the flexibility of marking the sweeps during the examination.

RESULTS

After grouping the B-scans into sweeps, a voxel array can be reconstructed for each sweep using the algorithm in Fig. 4. At this stage, it is possible to appreciate the registration errors by viewing corresponding slices through the reconstructions (see Fig. 9). Compounding the sweeps using the position measurements alone gives unsatisfactory results, as can be seen in Fig. 10. Clearly, image-based registration is essential for accurate spatial compounding.

The first stage of registration is the calculation of the gradients. Gradients calculated at both 2-mm and

Fig. 17. 3-D segmentation of compounded reconstruction after data processing. This image is produced in the same manner as Fig. 16. Spatial compounding improves the organ segmentation. Compared to the segmentation of the individual sweeps, the compounded data set is the only one in which the gall bladder is completely disconnected from surrounding noise and artifacts. Complete isolation of the gall bladder is now easily performed (see Fig. 18).

1-mm resolutions are shown in Fig. 11a, b. The scale of the gradient operator was chosen to minimise the effect of speckle, yet retain the features of the anatomical structures. The correlation calculations were performed on a Silicon Graphics Indigo 2 Impact 10000 workstation, Silicon Graphics Corporation, Mountain View, California taking 3.6 h per sweep. This includes calculation of the gradients and the two searches at both resolutions. Although this is undoubtedly expensive, the procedure is readily parallelised and the times are comparable to those accepted for CT and MRI registration (van den Elsen et al. 1995). The registration results for each sweep are listed in Table 1.

Slices of the registered and compounded data set are shown in Fig. 12. The borders of the gall bladder are all well aligned, compared to the unregistered case in Fig. 10. The level of speckle noise is also reduced compared to the single-sweep reconstructions of Fig. 9. Furthermore, the organ boundaries of the registered and compounded reconstruction have better contrast and are more uniform than in the single-sweep reconstructions. Although all of these improvements are benefits of spatial compounding, it has to be admitted that, on close inspection, a slight loss of spatial detail is apparent. The residual registration errors that are not corrected (such as nonrigid motion of the organ and local refraction of the ultrasound beam) result in a slight blurring of small features. The main benefits of spatial compounding are, therefore, improved segmentation and visualisation of larger structures.

Segmentation, the process of separating a particular anatomical region of interest from the surrounding data, is a key step in visualisation and volume estimation. Perfect segmentation of the gall bladder requires that all parts of the organ be accurately identified and no regions outside the organ be included.

To objectively compare the quality of the compounded reconstruction with the single-sweep reconstructions, automatic segmentation by intensity thresholding was attempted. Figures 13 and 14 show how spatial compounding improves the ability to segment by thresholding. Essentially, spatial compounding has the ability to fill in regions that are not well-defined in some sweeps, but are clearer in others. Note that this improvement is not achievable by filtering, which introduces no new information.

The reduction of speckle noise by spatial compounding is difficult to see in the reconstruction slices. It is more clearly evident in 3-D surface renderings of original (unprocessed) 3-D data sets. Figure 15a, b shows a significant amount of speckle reduction by spatial compounding. The compounding allows a significant fraction of the gall bladder surface to be viewed without any filtering.

Further improvements are possible with a small amount of data processing before segmentation and rendering. A typical ultrasound visualisation procedure involves interpolating and filtering the data before surface detection is attempted (Nelson and Elvins 1993; Sakas et al. 1995). Figure 16a–f shows that interpolation and filtering of single-sweep reconstructions improves visu-

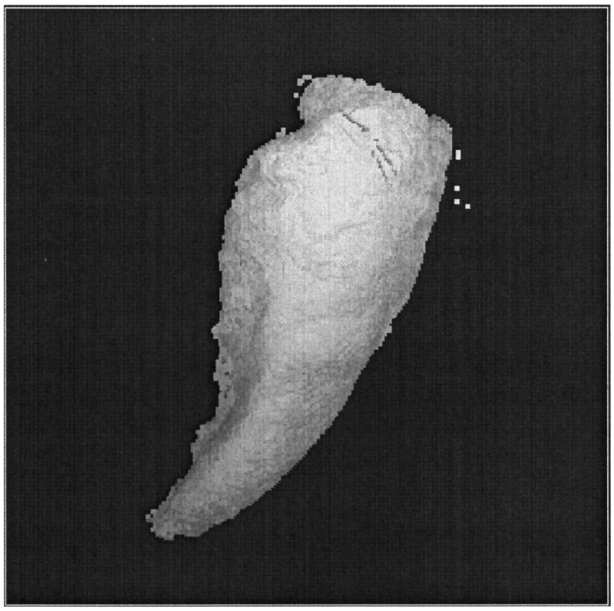

Fig. 18. 3-D segmentation of high-resolution compounded reconstruction. This image is produced from a high resolution reconstruction compounded with Sweeps 0 to 5. The data is first interpolated, median filtered, threshold segmented, then manually trimmed of extraneous regions.

Table 2. Volume of gall bladder.

Sweep	Volume (mL)
0	13.494
1	16.662
2	15.758
3	14.945
4	15.117
5	14.166
Compounded	13.039
Live-wire	12.507

The compounded data set provides the volume estimate closest to the ''gold standard'' live-wire segmentation.

alisation, but problems still remain. The main problem is that ill-defined boundaries (like the ones in Fig. 13) are not improved by interpolation and filtering. The segmentation does not isolate the gall bladder from the surrounding noise and artifacts in single-sweep reconstructions. Performing the same data processing on the registered and compounded data does isolate the gall bladder, as shown in Fig. 17. Removal of the unwanted, disconnected regions becomes a trivial task, with the results shown in Fig. 18.

Organ volume is a measure that is often sought by physicians. Measuring changes in the volume of an organ over time is often used to monitor the progression of a disease or its response to treatment. For example, it is useful to measure the reduction in prostate size during reductase inhibitor therapy, and changes in splenic size during enzyme replacement therapy for Gaucher's disease. There is also a need to measure changes in the size of uterine leiomyomas (fibroids) in response to treatment by luteinising hormone-releasing hormone antagonists.

Volume estimation follows a similar trend to visualisation because both rely upon accurate segmentation. Because the true volume of the gall bladder is unknown, we chose to use live-wire semi-automatic segmentation (Barrett and Mortensen 1996) of the baseline sweep as a "gold standard." Live-wire segmentation is a powerful tool for extracting boundaries in noisy images. It offers a good compromise between accuracy and amount of user intervention. The technique involves laying an active wire around the object on a slice-by-slice basis. The wire is attracted automatically to the object's boundary. The operator assists the live-wire by depositing small sections at a time near the boundary, so that the wire does not enclose nearby speckle.

In addition to the live-wire estimate, volumes for individual sweeps and the compounded reconstruction were calculated using the same process (interpolation, filtering and thresholding) used for the visualisation results in Figs. 16 and 17. To calculate only the gall bladder volume, any segmented part of the data that was not connected to the gall bladder was removed manually. The volume was then calculated by summing the remaining filled voxels that contained the segmented gall bladder.

The calculated volume of the compounded data is closer to the live-wire estimate than any of the individual sweeps (see Table 2). The volumes for each of the individual sweeps were higher than the live-wire volume because the segmentation of the gall bladder typically exceeds the gall bladder boundary (as evident in Fig. 13). This again shows that segmentation of spatially compounded data sets gives better results than single sweeps.

CONCLUSIONS AND FUTURE WORK

Ultrasound data is more difficult to register than data from other modalities, such as MRI and CT. We have demonstrated, for the first time, the registration of 3-D ultrasound data using a technique developed for MRI to CT registration. The registration technique was chosen according to the particular requirements of ultrasound data.

Registration was performed in a fully automatic manner, eliminating user subjectivity. The registration is based on the correlation of features obtained by calculation of the 3-D gradient, so neither explicit segmentation nor landmark identification is required. Implementation of the registration technique on *in vivo* ultrasound data has shown it to be robust and accurate. The efficiency of the algorithm is also improved via a multiresolution search for the correlation peak.

The main application we have considered in this paper is spatial compounding. We used a freehand ultrasound acquisition system that can acquire many overlapping B-scans in a short period of time. The rapid acquisition allows spatial compounding of multiple 3-D data sets obtained from different views of the same organ during a single examination.

Although system calibration is performed prior to each examination, registration errors remain in the 3-D data sets. Accurate spatial compounding requires correc-

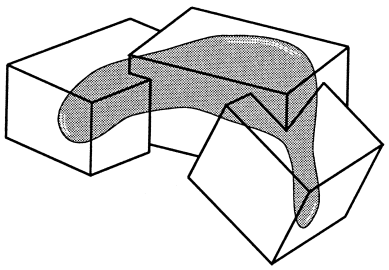

Fig. 19. Extended volume of interest. Several small, partially overlapping volumes can be combined to encompass a larger organ.

tion of the errors by image-based registration. We have shown that rigid body registration is sufficient to correct a large proportion of the registration errors. Because the registration errors are known to be small, registration by correlation is feasible by searching a small portion of the 6-D parameter space.

The resulting registered and compounded 3-D data sets offer improved segmentation for better visualisation and volume estimation. Application of state-of-the-art visualisation techniques to the compounded data has produced dramatically clear and accurate images of the gall bladder. Other users of 3-D ultrasound can use the techniques described in this paper, because they can be applied to any regular 3-D ultrasound data sets, independent of the particular method of data acquisition.

Because correlation-based registration can register volumes that are only partially overlapping, it is possible to combine several small volumes of data to form a larger volume. An example is shown in Fig. 19. Accurate registration of the overlapping volumes will be required to avoid discontinuities in the data. This concept is especially useful for data-acquisition systems that can examine only small volumes at a time, such as the commercially available Voluson 530D system (Kretztechnik AG, Zipf, Austria).

Many conventional ultrasound scanners are also capable of producing Doppler ultrasound images. In Doppler ultrasound, pulse-echo information can be used to calculate the speed of fluids passing through vessels, providing important vascular flow information. Although Doppler ultrasound can provide information no other imaging modality can, it suffers from considerable signal dropout and noise. Spatial compounding of 3-D Doppler ultrasound data is another very promising direction for future research.

Acknowledgements—Calculations of the 3-D gradients were performed by a separable, recursive 3-D edge detector, kindly provided by the researchers at INRIA, Sophia Antipolis, France. The freehand acquisition system was developed by Richard Prager and Patrick Gosling, and the 3-D renderings were produced using the 3DViewnix® visualisation package. Robert Rohling is supported by Churchill College and an ORS award.

REFERENCES

Barrett W, Mortensen E. Fast, accurate, and reproducible live-wire boundary extraction. In: Hohne K, Kikinis R, eds. Lecture notes in computer science: visualization in biomedical computing. Proc VBC '96. vol. 1131. Heidelberg, Germany: Springer-Verlag, 1996; 183–192.

Carr J. Surface reconstruction in 3D medical imaging. Ph.D. Thesis, University of Canterbury. Christchurch, New Zealand, 1996.

Chervenak F, Isaacson G, Campbell S. Ultrasound in obstetrics and gynecology. Boston, MA: Little, Brown and Company, 1993.

Deng J, Gardener JE, Rodeck CH, Lees WR. Fetal echocardiography in 3-dimensions and 4-dimensions. Ultrasound Med Biol 1996;22: 979–986.

Fenster A, Downey DB. 3-D ultrasound imaging—a review. IEEE Eng Med Biol Mag 1996;15:41–51.

Fine D, Perring S, Herbetko J, et al. Three-dimensional (3D) ultrasound imaging of the gallbladder and dilated biliary tree: reconstruction from real-time B-scans. Br J Radiol 1991;64:1056–1057.

Franceschi D, Bondi JA, Rubin JR. A new approach for three-dimensional reconstruction of arterial ultrasonography. J Vasc Surg 1992; 15:800–805.

Gilja OH, Smievoll AI, Thune N, et al. In vivo comparison of 3D ultrasonography and magnetic resonance imaging in volume estimation of human kidneys. Ultrasound Med Biol 1995;21:25–32.

Hottier F, Collet Billon A. 3D echography: status and perspective. In: Hohne K, Fuchs H, Pizer S, eds. 3D imaging in medicine: algorithms, systems, applications. Berlin, Germany: Springer-Verlag, 1990:21–41.

Levine DN, Pelizzari CA, Chen GTY, Chen CT, Cooper MD. Retrospective geometric correlation of MR, CT and PET images. Radiology 1988;169:817–823.

Maintz JBA, van den Elsen PA, Viergever MA. Comparison of edge-based and ridge-based registration of CT and MR brain images. Med Image Anal 1996;1:151–161.

Monga O, Deriche R, Malandain G, Cocquerez JP. Recursive filtering and edge tracking: two primary tools for 3-D edge detection. Image Vision Comput 1991;9:203–214.

Moskalik A, Carson PL, Meyer CR, et al. Registration of three-dimensional compound ultrasound scans of the breast for refraction and motion correction. Ultrasound Med Biol 1995;21:769–778.

Nelson T, Pretorius D. 3D ultrasound image quality improvement using spatial compounding and 3D filtering. Med Phys 1994;21:998.

Nelson TR, Elvins TT. Visualization of 3D ultrasound data. IEEE Comput Graphics Applic 1993;13:50–57.

Rohling R, Gee A, Berman L. 3-D spatial compounding of ultrasound images. Med Image Anal 1997;1:177–193.

Sakas G, Schreyer LA, Grimm M. Preprocessing and volume rendering of 3D ultrasonic data. IEEE Comput Graphics Applic 1995;15:47–54.

Salustri A, Roelandt JRTC. Ultrasonic three-dimensional reconstruction of the heart. Ultrasound Med Biol 1995;21:281–293.

Smith SW, Davidsen RE, Emery CD, Goldberg RL, Light ED. Update on 2-D array transducers for medical ultrasound. Proc IEEE Ultrason Sympos 1995;2:1273–1278.

Steiner H, Staudach A, Spitzer D, Schaffer H. Three-dimensional ultrasound in obstetrics and gynaecology: technique, possibilities and limitations. Hum Reprod 1994;9:1773–1778.

Taylor RH, Lavallee S, Burdea GC, Mosges R, eds. Computer-integrated surgery. Cambridge, MA: MIT Press, 1996.

Thirion JP, Monga O, Benayoun S, Gueziec A, Ayache N. Automatic registration of 3D images using surface curvature. Conference on Mathematical Methods in Medical Imaging 1992:206–216.

van den Elsen P, Pol EJD, Viergever M. Medical image matching: a review with classification. IEEE Eng Med Biol Mag 1993;12:26–39.

van den Elsen PA, Maintz JBA, Pol EJD, Viergever MA. Automatic registration of CT and MR brain images using correlation of geometrical features. IEEE Trans Med Imaging 1995;14:384–396.

Wells PNT. Advances in ultrasound techniques and instrumentation. New York: Churchill Livingstone Inc, 1993. AU1: Please provide manufacturer and city, and state or country